# Microstructural evolution and thermal stability of 1050 commercial pure aluminum processed by high-strain-rate deformation

Yang Yang
*School of Material Science and Engineering, Central South University, Changsha 410083, China; Institute of Fluid Physics, China Academy of Engineering Physics, Mianyang 621900, China; State Key Laboratory of Explosion Science and Technology, Beijing Institute of Technology, Beijing 100081, China; and Key Laboratory of Ministry of Education for Nonferrous Metal Materials Science and Engineering, Central South University, Changsha 410083, China*

Ya Dong Chen[a)]
*School of Material Science and Engineering, Central South University, Changsha 410083, China*

Hai Bo Hu and Tie Gang Tang
*Institute of Fluid Physics, China Academy of Engineering Physics, Mianyang 621900, China*

Ren Rong Long and Qing Ming Zhang
*State Key Laboratory of Explosion Science and Technology, Beijing Institute of Technology, Beijing 100081, China*

(Received 4 May 2015; accepted 8 October 2015)

Microstructural and property evolution of 1050 commercial pure aluminum subjected to high-strain-rate deformation (1.2–2.3 $\times$ $10^3$ $s^{-1}$) by split Hopkinson pressure bar (SHPB) and subsequent annealing treatment were investigated. The as-deformed and their annealed samples at 373–523 K were characterized by transmission electron microscopy (TEM) and microhardness tests. TEM observations reveal that the as-deformed sample is mainly composed of a lamellar structure, whose transverse/longitudinal average subgrain/cell sizes are 293 and 694 nm, respectively. The initial coarse grains are refined significantly. The initial lamellar grain structures are subdivided into pancake-shaped subgrains due to a gradual transition by triple junction motion at 473 K, and then a dramatic microstructural coarsening is observed at 523 K. It is suggested that annealing behavior of this dynamic loading structure is better considered as a continuous process of grain coarsening or continuous recovery.

## I. INTRODUCTION

Pure aluminum and aluminum alloys play a key role in modern engineering since they are the most used nonferrous materials. They have been widely used in automotive, aerospace, and construction engineering due to their good corrosion resistance, superior mechanical properties along with good machinability, weldability, and relatively low cost. It is well known that the grain size is one of the principal tools for controlling mechanical properties of polycrystalline metallic materials. At low temperatures, the yield strength is related to the grain size by the well-known Hall–Petch relationship, where the yield strength of the material increases with decreasing grain size. Currently, there are several commonly used methods of refining grains in laboratory, such as power deposition,[1] severe plastic deformation (SPD),[1] and dynamic plastic deformation (DPD).[2,3]

As the competition between the generation and the annihilation of dislocations reaches a dynamic balance, a steady plastic deformation will occur. Experimental results indicated that the grain size has a linear relationship with the inverse square root of dislocation density ($D_c = K\rho^{-1/2}$).[4] Plenty of research showed that there is a saturate grain size during the SPD of metallic materials.[5] To refine grain further, some special methods should be developed, such as cryogenic or DPD.[6,7]

Ultrafine grain materials that were produced by SPD or DPD contain a large amount of dislocations and nonequilibrium grain boundaries, which result in significant increase in hardness and strength but limited stability.[8–11] That is to say, such microstructures can be easily changed by recovery and recrystallization during annealing. Microstructural coarsening will inevitably weaken mechanical properties of materials, against their application as potential engineering materials. Therefore, it is essential to clarify the coincident influences of annealing treatment on the microstructural evolution, along with reducing the instabilities.

1050 commercial pure aluminum was subjected to high-strain-rate deformation with the strain rate up to 2.3 $\times$ $10^3$ $s^{-1}$ by means of split Hopkinson pressure bar (SHPB) in this work. The effects of the high strain rate on microstructural evolution and thermal stability of 1050 commercial pure aluminum were investigated.

Contributing Editor: Andrea Maria Hodge
[a)]Address all correspondence to this author.
e-mail: yadongchen1990@163.com
DOI: 10.1557/jmr.2015.341

 © Materials Research Society 2015

https://doi.org/10.1557/jmr.2015.341 Published online by Cambridge University Press

## II. MATERIALS AND METHODS

1050 commercial pure aluminum (0.25% Si, 0.05% Mn, 0.05% Cu, 0.05% Mg, 0.05% Zn, and the balance Al, all in mass percentage) was annealed at 673 K for 3 h in a salt-bath furnace to diminish the effect of residual stress and obtain homogeneous coarse grains. The average grain size of these samples is about 46 μm. The cylindrical samples (Φ15 mm × 23 mm) were prepared for uni-axial impact loading.

Figure 1 is the schematic diagram of SHPB, which was originally developed by Kolsky.[12] The cylindrical-shaped samples (Φ15 mm × 23 mm) were prepared for uni-axial impact loading at high strain rates, and a reduction about 40% was achieved per pass. Plastic strain obtained during each pass is defined as $\varepsilon = \ln(h_0/h_f)$, where $h_0$ and $h_f$ are the initial and the final thickness. The accumulation strain of uni-axial impacted samples was 1.8. The samples for annealing treatment were cut parallel to the loading direction, then annealed at 373, 423, 473, and 523 K for 1 h and quenched in water.

Microstructures of the as-deformed and annealed samples were characterized by using a Titan G2 60-300 transmission electron microscope (TEM; FEI Company, Eindhoven, Netherlands) in a section that is parallel to the loading direction, i.e., the longitudinal section. Thin foils for TEM observations were prepared by mechanical grinding to a thickness of 60 μm, final electro-polishing at 253 K in an electrolyte of 30% nitric acid and 70% methanol with a Struers Tenupol-5 double jet electro-chemical machine (Struers, Ballerup, Denmark) operating at 20 V was carried out. Microhardness measurements were conducted on the longitudinal section under 3 kg load for 15 s. At least six separate measurements were conducted for each hardness value.

## III. EXPERIMENT RESULTS

### A. Flow stress–strain response

The signals of SHPB are electrical, as shown in Fig. 2 (the black solid line and red solid line represent the signals of the incident bar and transmitter bar, respectively), which should be transformed into mechanical information by the classical SHPB equation[2,3]:

$$\varepsilon = -2C_0 \Big/ L_0 \int_0^t \varepsilon_r \, dt \quad , \tag{1}$$

$$\dot{\varepsilon} = d\varepsilon/dt = -2C_0\varepsilon_r/L_0 \quad , \tag{2}$$

$$\sigma = EA_0\varepsilon_t/A \quad , \tag{3}$$

where $C_0$ and $E$ are the elastic wave velocity and elasticity modulus of pressure bar, respectively, $L_0$ is length of the sample before impact, $A_0$ and $A$ are cross-sectional areas of the pressure bar and sample before impact, $\varepsilon_r$ and $\varepsilon_t$ are electrical signals of the incident bar and transmitter bar, respectively. Strain rate–time ($\dot{\varepsilon} - t$) curves and stress–strain ($\sigma$–$\varepsilon$) relationships during high-strain-rate deformation are shown in Figs. 3(a) and 3(b).

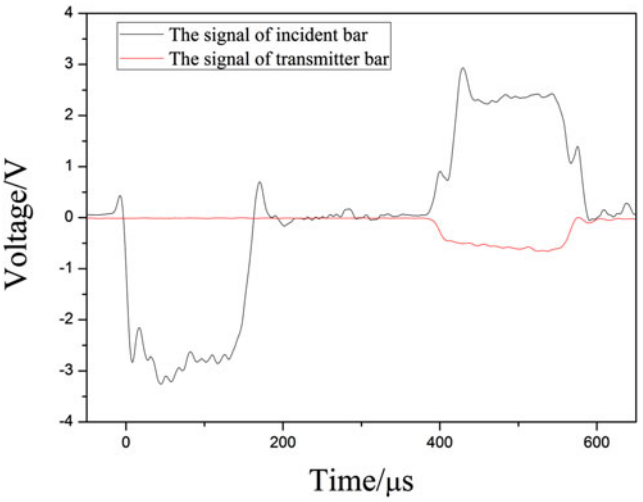



FIG. 2. The electrical signals of SHPB.

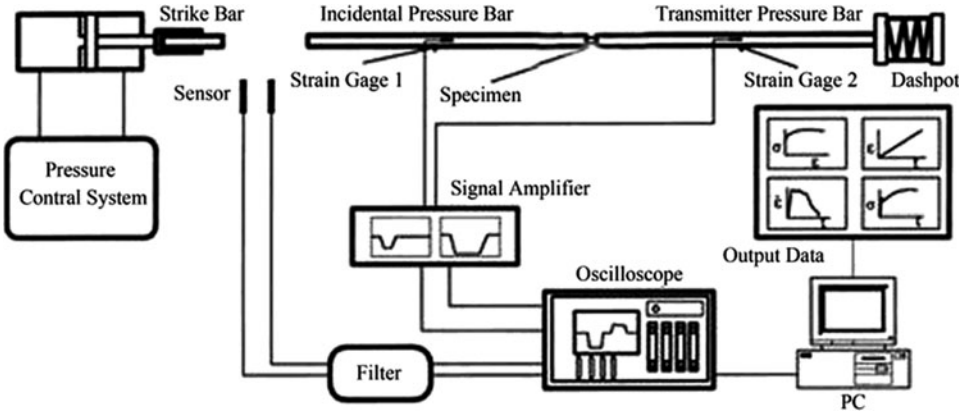



FIG. 1. Schematic diagram of SHPB.

https://doi.org/10.1557/jmr.2015.341 Published online by Cambridge University Press

In the process of uni-axial impact loading, the strain rate increases from 1200 $s^{-1}$ in pass 1 to 2300 $s^{-1}$ in pass 3, and the flow stress presents a similar trend. In the first two passes, the flow stress increases with increasing strain, which indicates the effect of strain hardening and strain rate hardening. There is a saturate flow stress in pass 3 and pass 4, being about 180 MPa, indicating a dynamic equilibrium between generation and annihilation of strain-induced dislocations.

### B. Microstructural characteristics of the samples after high-strain-rate deformation

Figure 4 shows the typical TEM micrographs and the corresponding selected area electron diffraction patterns observed from the longitudinal section of the deformed samples. The dominant structural features of this high-strain-rate deformed Al are extended dislocation boundaries forming lamellar structures, which possess a regular shape with distinct and straight boundaries as well as a very high interior dislocation density. Different dislocation configurations, such as dislocation tangles and dislocation cells are produced [see Fig. 4]. The elongated lamellar structure in this uni-axial impacted sample seems like a bamboo structure obtained during cold rolling deformation, that is to say, serious deformed textures were produced, which can also be proven by the elongated diffraction spots in Fig. 4. The lamellar structure mainly consists of two types of boundaries, namely geometrically necessary boundaries (GNBs) and incidental dislocation boundaries (IDBs).[13,14] High density of dislocations was generated during high-strain-rate deformation, and they tend to distribute uniformly within the lamellar structures.

For quantitative analysis of subgrain/cell size distribution, the spacings between GNBs ($D_T$) and IDBs ($D_L$) were measured from TEM images as the intercept length along a line perpendicular and parallel to the extending direction. The results are plotted in Fig. 5. Statistical measurements of the average subgrain/cell sizes from at least 150 grains/cells are 293 nm ($D_T$) and 694 nm ($D_L$), respectively.

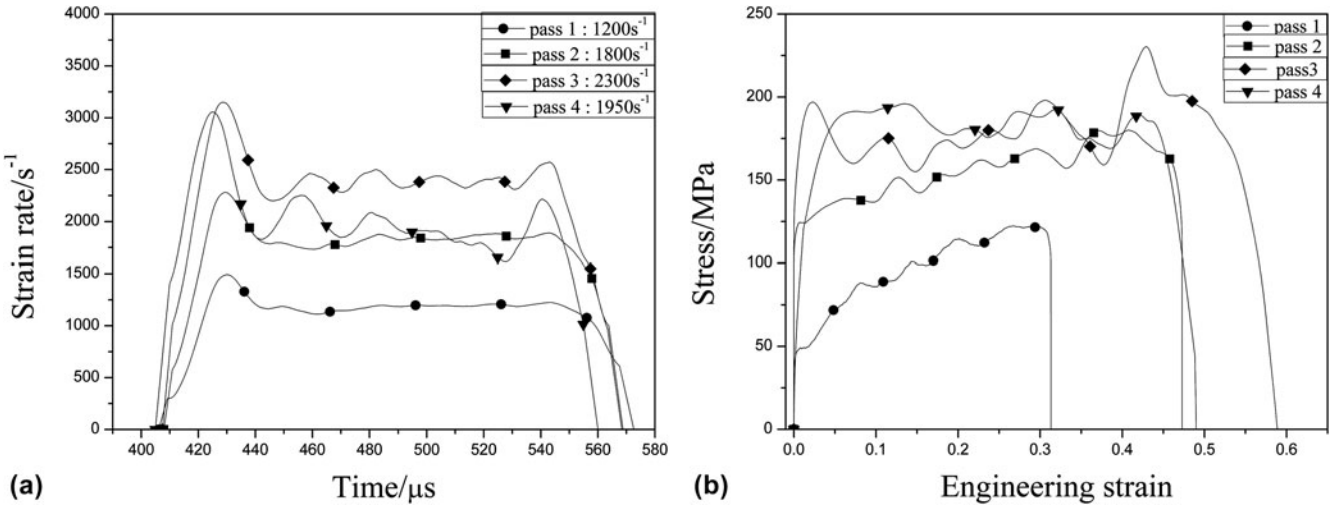



FIG. 3. (a) The strain rate–time curves and (b) stress–strain curves obtained during high-strain-rate deformation.

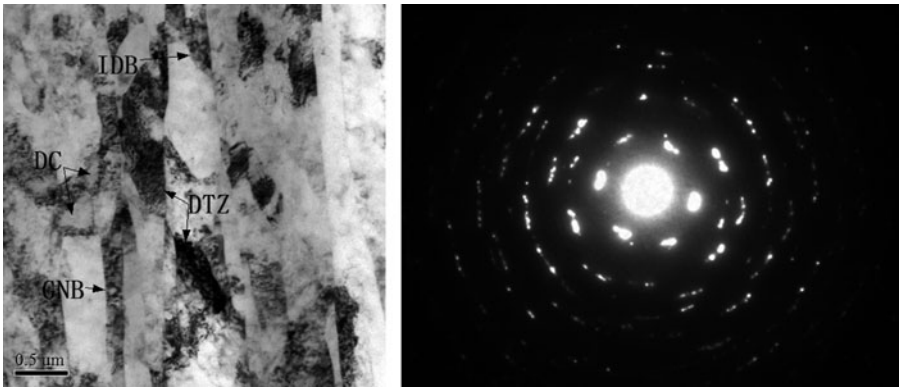



FIG. 4. TEM image of the as-deformed sample. The illustration is the selected area diffraction pattern.



https://doi.org/10.1557/jmr.2015.341 Published online by Cambridge University Press

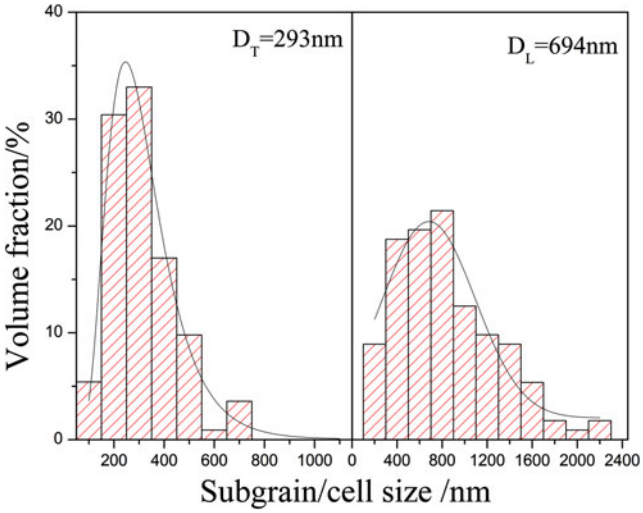



FIG. 5. Statistical distribution of subgrain/cell sizes. $D_T$ and $D_L$ are the spacings between GNBs and IDBs of the as-deformed samples.

### C. Microstructural evolution of the as-deformed samples during annealing treatment

Isochronal annealing treatments for 1 h at increasing temperature lead to softening, microstructural coarsening, and a change in the crystallographic morphology. Figure 6 shows the representative TEM images of the specimens annealed at temperatures from 373 to 523 K for 1 h. The microstructural coarsening of the specimens annealed below 423 K [Figs. 6(a) and 6(b)] is insignificant. The majority of crystallites is still elongated. However, a mild microstructural coarsening is observed after annealing at 473 K [Fig. 6(c)]. The elongated lamellar structures are subdivided into subgrains. Most of the subgrains are pancake-shaped and consist of a large number of dislocations in the interior. Figure 6(d) shows that the microstructural features drastically change after annealing at 523 K for 1 h, and a significant microstructural coarsening and sharp grain boundaries evolve.

Statistical distribution of subgrain/cell sizes from at least 150 subgrains/cells of the sample annealed below 473 K exhibits a lognormal distribution. Migration and interaction of the interior dislocations result in formation of incident dislocation boundaries and segmentation of lamellar structures into fine subgrains below 423 K, and thus $D_L$ decreases. For the sample annealed at 473 K [Fig. 7(c)], $D_T$ and $D_L$ are 442 and 875 nm, respectively, which coarsen slightly when compared with those annealed below 423 K. However, the sample with an average grain size of 4.7 μm was produced after annealing at 523 K for 1 h [Fig. 7(d)].

### D. Microhardness measurements

The specimens for microhardness tests are sectioned parallel to the loading direction from the as-deformed samples and the annealed samples, and the results are illustrated in Fig. 8. The microhardness gradually decreases with increasing annealing temperature at low temperatures below 473 K, which has been interpreted as continuous recovery or recrystallization at temperature above 473 K.

## IV. DISCUSSION

### A. Flow stress curve characteristics

As shown in Fig. 3(b), the flow stress increases with the increasing strain in pass 1 and pass 2, indicating the effect of strain and strain rate hardening in the process of high-strain-rate deformation. There is a saturate flow stress in pass 3 and pass 4, the effect of work hardening is insignificant at large strains, which is attributed to generation and annihilation of dislocations reaching an equilibrium state. Besides, the saturate flow stress of commercial-pure aluminum in this work is about 190 MPa, larger than that of experiment results of quasistatic loading 120–170 MPa (see Refs. 15–18). It is therefore to be expected that higher density of crystal defects (mainly dislocations) introduced by high strain rate loading is responsible for this higher flow stress.

### B. Microstructural evolution mechanism during high-strain-rate deformation

Figure 4 shows that the structural morphology appears not to be strongly affected by the increase in the strain rate and the dominating deformation mechanism in this high-strain-rate deformed Al is typically dislocation glide. The universal pattern of microstructural evolution during deformation at a low strain rate also applies when the strain rate is increased to a high level of $10^3$ $s^{-1}$. However, the mechanism of dislocation nucleation is clearly affected by the significant increase in the strain rate.

It is well known that the dislocation nucleation mechanism in the process of quasistatic plastic deformation can be explained by the Frank–Read source model. While for deformation at an extremely high strain rate, the homogeneous dislocation nucleation mechanism proposed by Meyers[2] is applicable.

In light of the above model, during DPD, stress propagates along the loading direction in the form of a wave. As the shock wave penetrates into the material, high deviatoric stresses effectively distort the initially cubic lattice into a monoclinic lattice. When these stresses reach a certain threshold level, homogeneous dislocation nucleation can take place and then high densities of uniformly distributed dislocations are generated. Meanwhile, dislocations propagate at a speed of subsonic, but the propagation distance is limited. In general, the density of dislocation produced under high-strain-rate loading is about $10^3$–$10^4$ times higher than that under statics loading.[2]

https://doi.org/10.1557/jmr.2015.341 Published online by Cambridge University Press

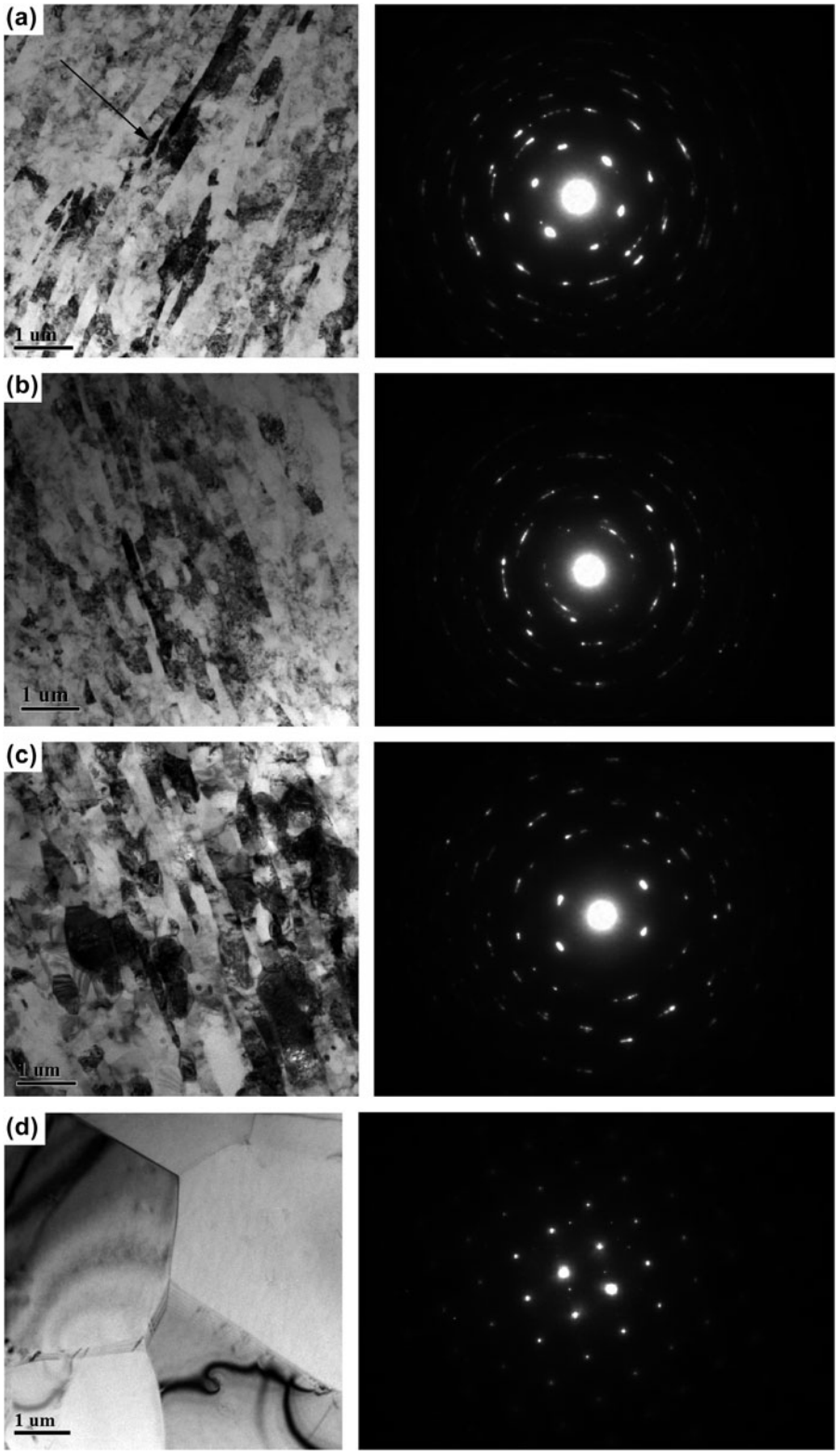



FIG. 6. TEM images of the as-deformed specimens after 1 h annealing at various temperatures and the black arrow indicates the loading direction. (a) 373 K, (b) 423 K, (c) 473 K, and (d) 523 K.

For the short loading periods during high-strain-rate deformation at $10^3$ $s^{-1}$, dislocation movement and interactions are restricted, resulting in the limited motion distance of dislocations, so dislocation density is significantly higher than conditions of quasistatic loading. Density of dislocations can be approximated as given in Eq. (4) (Ref. 19):



https://doi.org/10.1557/jmr.2015.341 Published online by Cambridge University Press

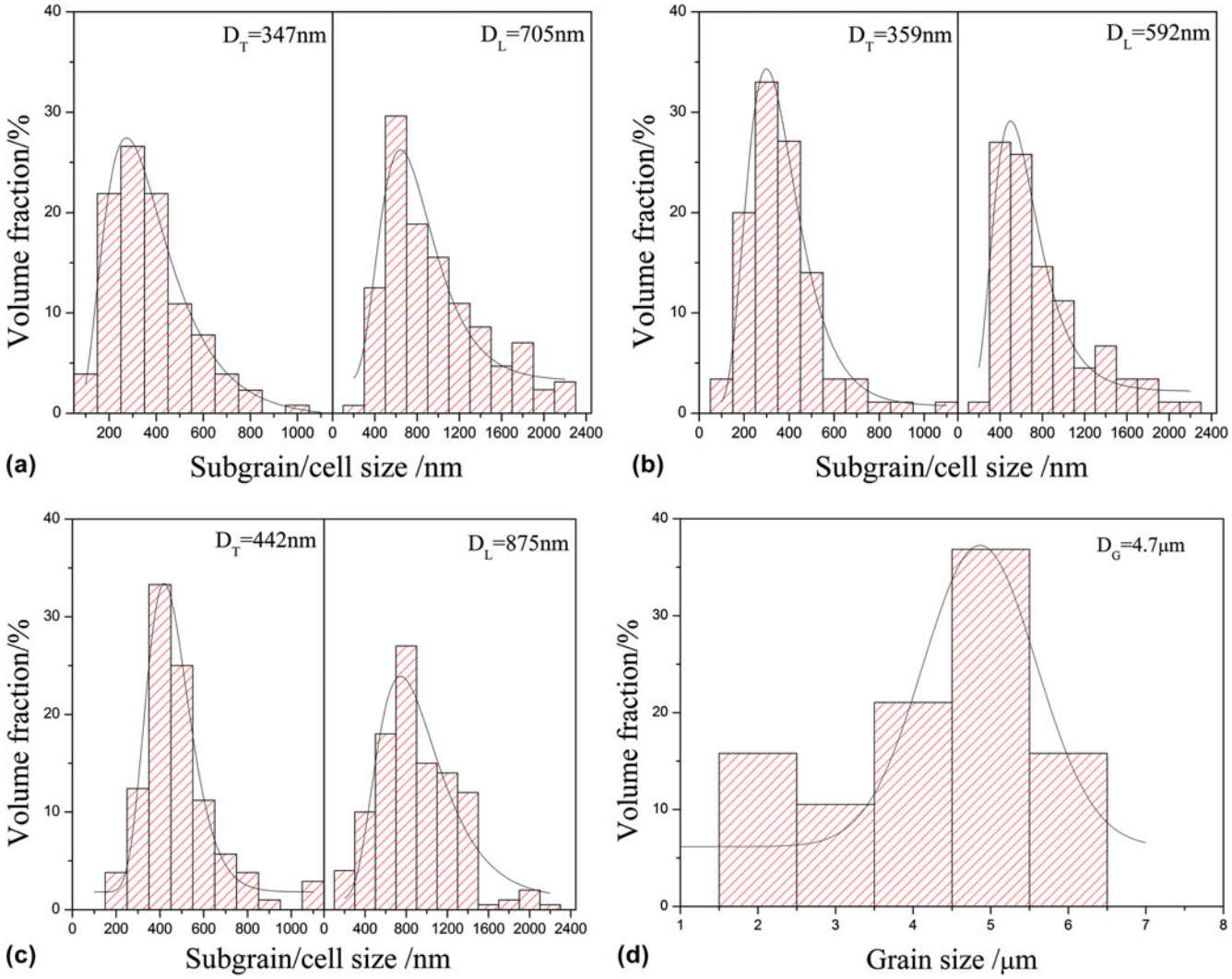



FIG. 7. Statistical distribution of subgrain/cell sizes. (a)–(c) are the spacings between GNBs ($D_T$) and IDBs ($D_L$) of the samples after 1 h annealing treatment at 373, 423, and 473 K, respectively; (d) is the grain size distribution of the sample after 1 h annealing treatment at 523 K.

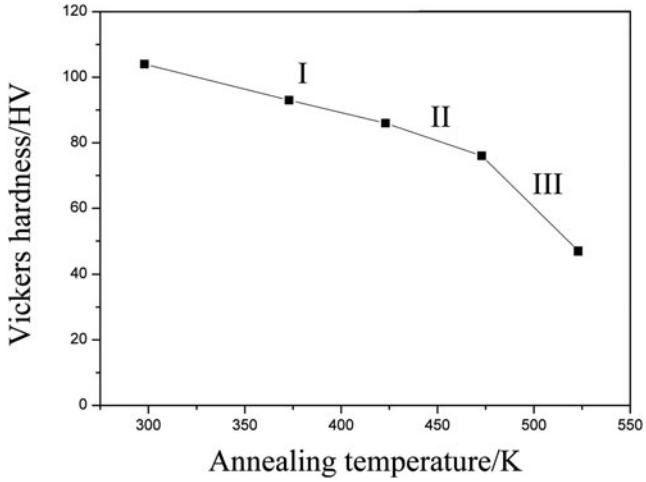



FIG. 8. Microhardness curve of the as-deformed samples as a function of annealing temperatures.

$$\dot{\gamma} = \rho b \upsilon \quad , \tag{4}$$

where $\dot{\gamma}$ is the shear strain rate, ρ is average density of mobile dislocation per unit volume, $v$ is the dislocation velocity, and $b$ is the Burgers vector. During DPD, a higher strain rate is beneficial for the generation of dislocations, while the rearrangement and annihilation of dislocations are depressed and the average free path of mobile dislocation is limited, which results in a higher density of dislocations. Therefore, high-strain-rate deformation is significantly beneficial for the efficient refinement of grains according to the above qualitative analysis.

The average grain sizes of pure aluminum produced by different technologies are listed in Table I. It can be seen that a similar effect of grain refining has been obtained, but the accumulate strain of dynamic loading in this work is significantly lower than that of quasistatic loading, thus

https://doi.org/10.1557/jmr.2015.341 Published online by Cambridge University Press

TABLE I. The average grain sizes of pure aluminum produced by different technologies.

| Materials | Deformation style | Accumulated strain | $D_T$ (nm) | $D_L$ (nm) |
|---|---|---|---|---|
| A1050 | SHPB | 1.8 | 293 | 694 [Present work] |
| 1100-Al | ARB | 4.8 | 270 | 1200 (Ref. 16) |
| A1050 | ECAE | 8.0 | 350 | 600 (Ref. 20) |
| Al (99.5%) | CR | 1.4 | 250–350 | 500–1000 (Ref. 21) |

ARB = Accumulative Roll Bonding, ECAE = Equal Channel Angular Extrusion, CR = Cold Rolling.

one can say that dynamic loading is more beneficial for the efficient refinement of grains than quasistatic loading under the same strain.

### C. Thermal stability of the as-deformed structure

Yu et al.,[20] Mishin et al.[22] and Hansen et al.[23] found that annealing treatment of cold rolled aluminum alloys has led to a possible change from conventional (discontinuous) recrystallization at low-to-medium strains to extended recovery or continuous recrystallization at very large strains. In this work, the initial lamellar grain structures of a dynamic impacted sample which consists of elongated grains are subdivided into pancake-shaped subgrains due to a gradual transition by triple junction motion[24] at 473 K, and then a dramatic microstructural coarsening is observed at 523 K.

With the assumption that the driving force on a boundary arises only from the curvature of the boundary, the kinetics of grain growth can be described by Eqs. (5) and (6) (Ref. 25):

$$D^2 - D_0{}^2 = kt^n \quad , \tag{5}$$

$$k = A\,\exp(-Q/RT) \quad , \tag{6}$$

where $D$ is the average grain size at time $t$ (here taken as the equivalent circle diameter, the diameter of a circle having the same area as the grain, $D_T \times D_L = \pi D^2/4$), $D_0$ is the initial average grain size, $Q$ is the apparent activation energy for grain growth, $R$ is the gas constant, $T$ is the absolute temperature, and $A$ and $n$ are constants. For pure aluminum, the parameters $A$ and $n$ can be taken as $7.2 \times 10^{-12}$ m$^2$ and 1, respectively.[20,26] The average grain size obtained at different temperatures in the isochronal annealing treatment may be interpreted in terms of Eq. (5) by plotting $\log(D^2 - D_0{}^2)$ versus $1/T$, and the activation energy of grain growth can be determined. The result is shown in Fig. 9. At the annealing temperature below 473 K (regime I), the apparent activation energy is 51 kJ/mol, while in the range of 473–523 K (regime II), the apparent activation energy is 159 kJ/mol. Both were found to be much smaller than

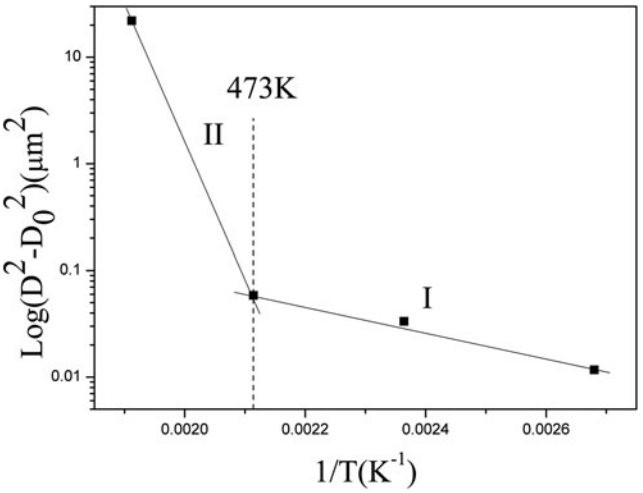



FIG. 9. The kinetics of grain growth is illustrated by plotting log $(D^2 - D_0{}^2)$ versus $1/T$. It shows a discontinuous transition from low-temperature (regime I) to high-temperature (regime II).

that of recrystallization, which is 178 kJ/mol.[27] In addition, the hardness after 1 h at 523 K ($47H_V$) is far from the hardness of a fully recrystallized Al 1050 ($20H_V$). Therefore, the annealing behavior of this dynamic loading structure is better considered as a continuous process of grain coarsening or continuous recovery.

Stored energy ($E_s$) will increase as the dislocation density increases according to Eq. (7) (Ref. 28) as follows:

$$E_s = K\rho G b^2 \quad , \tag{7}$$

where $K$ is a constant, $\rho$ is the average density of mobile dislocation per unit volume, $G$ is the shear modulus, and $b$ is the Burgers vector. Higher density of dislocations produced in the process of high-strain-rate deformation means higher stored energy and more nonequilibrium dislocation configurations, which will inevitably provide more driving force for recovery and recrystallization, and further cause significant microstructural coarsening in the subsequent annealing treatment.

## V. CONCLUSION

(1) An elongated lamellar structure with an average subgrain/cell size of 293 and 694 nm in the direction perpendicular and parallel, respectively, to the extending direction is produced by high-strain-rate deformation. The initial coarse grains are refined significantly.

(2) The initial lamellar grain structures are subdivided into pancake-shaped subgrains due to a gradual transition by triple junction motion at 473 K, and then a dramatic microstructural coarsening is observed at 523 K. Annealing behavior of this dynamic loading structure is better considered as a continuous process of grain coarsening or continuous recovery.

https://doi.org/10.1557/jmr.2015.341 Published online by Cambridge University Press

(3) Thermal stability of dynamic loading samples in this work is well at lower annealing temperatures below 473 K, but it gets worse suddenly when annealed at 523 K. Therefore, the microstructure of this high-strain-rate deformed pure aluminum is stable below 473 K.

## ACKNOWLEDGMENTS

This work is supported by the National Natural Science Foundation of China (No. 51274245), NSAF (No. U1330126), the Ph.D. Programs Foundation of Ministry of Education of China (No. 20120162130006), the Hunan Provincial Natural Science Foundation of China (No. 14JJ2011), and the key project of State Key Laboratory of Explosion Science and Technology (No. KFJJ11-1).

## REFERENCES

1. I. Sabirov, M.Y. Murashkin, and R.Z. Valiev: Nanostructured aluminum alloys produced by severe plastic deformation: New horizons in development. *Mater. Sci. Eng., A* **560**, 1 (2013).
2. M.A. Meyers: *Dynamic Behavior of Materials* (John Wiley & Sons, Inc., New York, 1994); pp. 405–408.
3. Y. Yang, F. Ma, and H.B. Hu: Microstructure evolution of 2195 Al-Li alloy subjected to high-strain-rate deformation. *Mater. Sci. Eng., A* **606**, 299 (2014).
4. D. Hull and D.J. Bacon: *Introduction to Dislocations*, 3rd ed. (Pergamon Press, Oxford, England, 1984); p. 257.
5. Y.J. Chen, Y.J. Li, J.C. Walmsley, S. Dumoulin, S.S. Gireesh, S. Armada, P.C. Skaret, and H.J. Roven: Quantitative analysis of grain refinement in titanium during equal channel angular pressing. *Scr. Mater.* **64**, 904 (2011).
6. F. Huang, N.R. Tao, and K. Lu: Effects of strain rate and deformation temperature on microstructures and hardness in plastically deformed pure aluminum. *J. Mater. Sci. Technol.* **27**, 1 (2011).
7. Y.S. Li, N.R. Tao, and K. Lu: Microstructural evolution and nanostructure formation in copper during dynamic plastic deformation at cryogenic temperature. *Acta Mater.* **56**, 230 (2008).
8. P.N. Rao, D. Singh, and R. Jayaganthan: Mechanical properties and microstructural evolution of Al 6061 alloy processed by multidirectional forging at liquid nitrogen temperature. *Mater. Des.* **56**, 97 (2014).
9. C.C. Koch: Optimization of strength and ductility in nanocrystalline and ultrafine grained metals. *Scr. Mater.* **49**, 657 (2003).
10. P.C. Millett, R.P. Selvam, and A. Saxena: Stabilizing nanocrystalline materials with dopants. *Acta Mater.* **55**, 2329 (2007).
11. M.R. Shankar, S. Chandrasekar, A.H. King, and W.D. Compton: Microstructure and stability of nanocrystalline aluminum 6061 created by large strain machining. *Acta Mater.* **53**, 4781 (2005).
12. H. Kolsky: An investigation of the mechanical properties of materials at very high rates of loading. *Proc. Phys. Soc., Sect. B* **62**, 676 (1949).
13. Q. Liu, D. Juul, and N. Hansen: Effect of grain orientation on deformation structure in cold-rolled polycrystalline aluminum. *Acta Mater.* **46**, 5819 (1998).
14. Z.P. Luo, H.W. Zhang, N. Hansen, and K. Lu: Quantification of the microstructures of high purity nickel subjected to dynamic plastic deformation. *Acta Mater.* **60**, 1322 (2012).
15. R. Kapoor, A. Sarkar, R. Yogi, S.K. Shekhawat, I. Samajdar, and J.K. Chakravartty: Softening of Al during multi-axial forging in a channel die. *Mater. Sci. Eng., A* **560**, 404 (2013).
16. N. Tsuji, Y. Ito, Y. Saito, and Y. Minamino: Strength and ductility of ultrafine grained aluminum and iron produced by ARB and annealing. *Scr. Mater.* **47**, 893 (2002).
17. N. Kamikawa, X. Huang, N. Tsuji, and N. Hansen: Strengthening mechanisms in nanostructured high-purity aluminum deformed to high strain and annealed. *Acta Mater.* **57**, 4198 (2009).
18. E.A. El-Danaf, M.S. Soliman, A.A. Almajid, and M.M. El-Rayes: Enhancement of mechanical properties and grain size refinement of commercial purity aluminum 1050 processed by ECAP. *Mater. Sci. Eng., A* **458**, 226 (2007).
19. R.W. Cahn and P. Haasen: *Physical Metallurgy*, 4th ed., Vol. **III** (North-Holland, The Netherlands, 1996); p. 1869.
20. C.Y. Yu, P.Y. Sun, P.W. Kao, and C.P. Chang: Evolution of microstructure during annealing of a severely deformed aluminum. *Mater. Sci. Eng., A* **366**, 310 (2004).
21. N. Rangaraju, T. Raghuram, B.V. Krishna, K.P. Rao, and P. Venugopal: Effect of cryo-rolling and annealing on microstructure and properties of commercial pure aluminum. *Mater. Sci. Eng., A* **398**, 246 (2005).
22. O.V. Mishin, A. Godfrey, D. Juul Jensen, and N. Hansen: Recovery and recrystallization in commercial purity aluminum cold rolled to an ultrahigh strain. *Acta Mater.* **61**, 5354 (2013).
23. N. Hansen, X. Huang, M.G. Moller, and A. Godfrey: Thermal stability of aluminum cold rolled to large strain. *J. Mater. Sci.* **43**, 6254 (2008).
24. T.B. Yu, N. Hansen, and X.X. Huang: Linking recovery and recrystallization through triple junction motion in aluminum cold rolled to a large strain. *Acta Mater.* **61**, 6577 (2013).
25. T. Fur, R. Oresund, and E. Nest: Subgrain growth in heavily deformed aluminum-experimental investigation and modelling treatment. *Acta Metall. Mater.* **43**, 2209 (1995).
26. F.X. Zhao, X.C. Xu, H.Q. Liu, and Y.L. Wang: Effect of annealing treatment on the microstructure and mechanical properties of ultrafine-grained aluminum. *Mater. Des.* **53**, 262 (2014).
27. R.A. Vandermeer and N. Hansen: Recovery kinetics of nanostructured aluminum: Model and experiment. *Acta Mater.* **56**, 5719 (2008).
28. A. Godfrey, W.Q. Cao, N. Hansen, and Q. Liu: Stored energy, microstructure, and flow stress of deformed metals. *Metall. Mater. Trans. A* **36**, 2371 (2005).

https://doi.org/10.1557/jmr.2015.341 Published online by Cambridge University Press